Article

Two-Stepwise Hierarchical Adaptive Threshold Method for Automatic Rapeseed Mapping over Jiangsu Using Harmonized Landsat/Sentinel-2

Shaomei Chen [1] , Zhaofu Li [1],* , Tingli Ji [1], Haiyan Zhao [1], Xiaosan Jiang [1], Xiang Gao [1], Jianjun Pan [1] and Wenmin Zhang [2]

[1]   College of Resources and Environmental Sciences, Nanjing Agricultural University, Nanjing 210095, China; 2020803203@stu.njau.edu.cn (S.C.); 2019103075@njau.edu.cn (T.J.); haiyanzhao@njau.edu.cn (H.Z.); gis@njau.edu.cn (X.J.); 2020039@njau.edu.cn (X.G.); jpan@njau.edu.cn (J.P.)
[2]   Department of Geosciences and Natural Resource Management, University of Copenhagen, 1350 Copenhagen, Denmark; wz@ign.ku.dk
*   Correspondence: lizhaofu@njau.edu.cn

Abstract: Rapeseed distribution mapping is a crucial issue for food and oil security, entertainment, and tourism development. Previous studies have used various remote sensing approaches to map rapeseed. However, the time-consuming and labor-intensive sample data used in these supervised classification methods greatly limit the development of large-scale mapping in rapeseed studies. Regarding threshold methods, some empirical thresholding methods still need sample data to select the optimal threshold value, and their accuracies decrease when a fixed threshold is applied in complex and diverse environments. This study first developed the Normalized Difference Rapeseed Index (NDRI), defined as the difference in green and short-wave infrared bands divided by their sum, to find a suitable feature to distinguish rapeseed from other types of crops. Next, a two-stepwise hierarchical adaptive thresholding (THAT) algorithm requiring no training data was used to automatically extract rapeseed in Xinghua. Finally, two adaptive thresholding methods of the standalone Otsu and Otsu with Canny Edge Detection (OCED) were used to extract rapeseed across Jiangsu province. The results show that (1) NDRI can separate rapeseed from other vegetation well; (2) the OCED-THAT method can accurately map rapeseed in Jiangsu with an overall accuracy (OA) of 0.9559 and a Kappa coefficient of 0.8569, and it performed better than the Otsu-THAT method; (3) the OCED-THAT method had a lower but acceptable accuracy than the Random Forest method (OA = 0.9806 and Kappa = 0.9391). This study indicates that the THAT model is a promising automatic method for mapping rapeseed.

Keywords: rapeseed mapping; adaptive thresholding method; normalized difference rapeseed index; Otsu thresholding method; canny edge detection; Harmonized Landsat/Sentinel-2

1. Introduction

Detailed and fine rapeseed distribution mapping is of great importance for three reasons. Firstly, rapeseed map products are not only significant for food and oil security (rapeseed is an oily crop providing edible oil for the increasing population [1,2]), but they are also meaningful for animal husbandry (rapeseed contains rich protein for animal feed [3]). Secondly, the distribution information of rapeseed is pivotal for further research, such as crop yield prediction and the assessment of climate change effects on agriculture, promoting the development of digital agriculture [4]. Thirdly, the beautiful yellow flowers of rapeseed fields provide resources for entertainment and tourism [5]; thus, rapeseed maps offer lots of details for decision makers to plan for tourism development.

Remote sensing techniques have been widely used in crop mapping because they are timely, labor-saving, and inexpensive in contrast with traditional field surveys [6,7].

Previous studies showed that the mapping of rapeseed attracts less attention than that of its counterparts (e.g., winter wheat and paddy rice) [2]. The challenges of rapeseed mapping include the following: similarity in spectral response between rapeseed and other vegetation [2], spectral mixing pixels due to patchy rapeseed fields [8], cloud contamination reducing effect observation times [5], and expensive training samples limiting large-scale studies [5,9,10].

Existing studies concerning rapeseed mapping can be divided into two categories. The first category comprises studies employing ensemble classification techniques, such as Random Forest (RF) and Support Vector Machine (SVM), using images taken during the flowering period [11–14]. For example, Meng et al. (2020) used all the cloud-free Sentinel-2 images to select the optimal temporal phases for winter wheat and rapeseed extraction in Zhongxiang, China [11]. This method has a high accuracy but depends on large amounts of training samples.

The second category comprises studies employing phenological-based threshold segmentation [9,15,16]. This method has been receiving increasing attention for automatic crop mapping because it has a promising accuracy with an empirical threshold [9,17–19]. Nevertheless, a fixed threshold requires some samples to choose an optimal threshold for the purpose of improving accuracy, which, in some studies, was not enough to meet the requirement of zero training samples [9,16–18], and in other studies, it was challenging to apply it in other areas because the accuracy decreased when the environment changed [20,21]. Therefore, in some cases, the threshold was manually intervened with to achieve better performance [22]. For instance, Ashourloo (2019) developed the Canola Index (CI) concerning near-infrared (NIR), red, and green bands for automatic rapeseed mapping, while its threshold was selected using an empirical method, which needed sample data to choose an optimal threshold when extending to testing sites [9]. Some adaptive threshold methods, such as the Otsu thresholding method originally used in image segmentation [23], have been introduced in other research fields. The Otsu thresholding method has become popular in remote sensing areas. For example, Zhang (2021) and Singh (2020) employed the Otsu with Canny Edge Detection (OCED) thresholding method to extract aquatic vegetation from water [20,22]. These methods are usually used to extract open water from land, aquatic vegetation from water, and glaciers from non-glaciers because the images can be simply divided into two parts: the object and the background [20,22]. Furthermore, objects and backgrounds have huge differences in spectral response, so a threshold can separate objects and backgrounds easily [22]. To the best of our knowledge, the adaptive thresholding method has not been applied in crop mapping to date, because crops share similarities in spectra, making it a challenge to determine a suitable threshold.

Regarding classification features, spectral and phenological characteristics form the hypothetical bases to discriminate crops [6,11,24]. The Normalized Difference Vegetation Index (NDVI), Enhanced Vegetation Index (EVI), and Soil-Adjusted Vegetation Index (SAVI) are major features in most staple crop-mapping studies [2,25]. Because the canopy of rapeseed differs greatly from that of other crops during the flowering stage, new taxonomic features are often mined for rapeseed in studies of rapeseed extraction. Wang (2018) developed the Ratio Oilseed Rape Colorimetric Index (RRCI) based on HSV transformation according to the principle that the color of rapeseed landscapes differs from that of other landscapes during the flowering period, and then a decision tree was employed for automatic rapeseed extraction using a uniform threshold in Hubei province [15]. D'Andrimont (2020) used the Normalized Difference Yellow Index (NDYI) concerning green and blue bands to extract rapeseed fields based on RF and then tracked the flowering date [10]. Veloso (2017) explored the temporal profile of NDVI and the radar backscatter of various crops, including rapeseed, to evaluate phenological characteristics for potential applications [26]. The results of their study suggest that radar and visible-near infrared are the major features in crop mapping. However, there is a significant lack of short-wave infrared (SWIR) bands in phenological features, with focus usually placed on visible-near infrared (vis-NIR) bands. The SWIR band is sensitive to water, and it can improve our

understanding of vegetation moisture content; thus, it may provide more information to identify specific crops [27,28].

The objective of this study was to automatically map rapeseed using a two-stepwise hierarchical adaptive threshold method. This was undertaken by developing an adaptive-threshold-based algorithm, which includes two key points: the optimal feature and the adaptive threshold. Accordingly, this study aimed to (1) determine the optimal rapeseed discrimination feature; (2) find a suitable adaptive threshold method; and (3) develop an automatic rapeseed mapping method based on the feature and the adaptive threshold method mentioned above and apply this method in Jiangsu Province on the Google Earth Engine (GEE) platform.

2. Materials

2.1. Study Area

As shown in Figure 1, Xinghua County and Jiangsu Province were chosen as the study sites. Xinghua County was the training area because the field data used to develop the method were collected in Xinghua County, and Jiangsu Province was the testing area in order to evaluate the robustness of the proposed approach in a large-scale region with a more complicated environment.
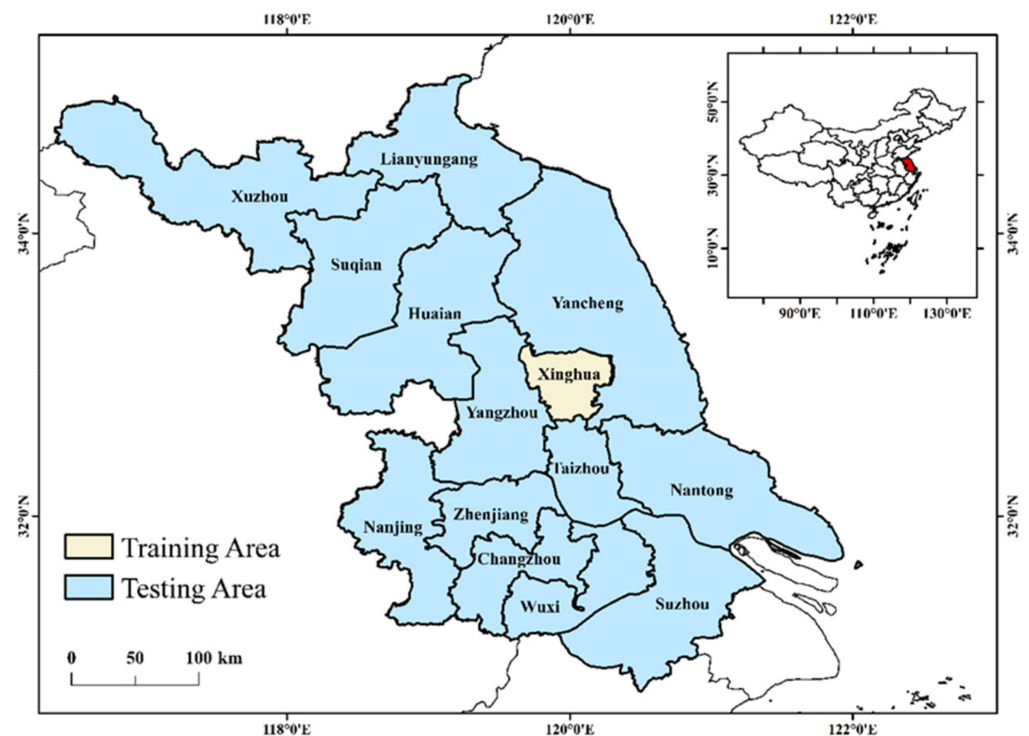

Figure 1. Location of study area, including training area, Xinghua County, and testing area, Jiangsu Province.

The location of Jiangsu Province is downstream of the Yangtze River (116°18′–121°57′ E, 30°45′–35°20′ N) [29], eastern China, covering an area of 102,600 km^2 [30]. Xinghua County has an area of 2393.35 km^2 and lies in the middle of Jiangsu Province, sharing a climatic environment and a crop planting structure with Jiangsu Province.

The climate type is a transition zone between subtropical and temperate monsoon climate zones, where the annual average temperature ranges from 13.6 to 16.1 °C, and the average annual precipitation is 1000 mm, which provides a suitable environment for agricultural development [31]. The summer crops in the study area are paddy rice, corn, and soybean; the winter crops are winter wheat and rapeseed. According to the situ survey, rapeseed is planted in a fragmented manner, mostly distributed on the ridge and

polder. The phenological calendar of rapeseed presented in Table 1 was collected from the Meteorological Bureau of Jiangsu Province.

Table 1. Phenological calendar of rapeseed in Jiangsu Province.

Month	Oct		Nov			Dec			Jan			Feb			Mar			Apr			May			Jun	
	II	III	I	II	III	I	II	III	I	II	III	I	II	III	I	II	III	I	II	III	I	II	III	I	II
Ten-day Phase																									

Seedling: blue; tillering: green; overwintering: gray; bolting: orange; flowering: yellow; pod filling: purple; harvesting: pink.

2.2. Sample Data Acquisition

The sample datasets were collected by conducting a field survey in Xinghua County in April and by visually interpreting high-resolution images, including those from Sentinel-2 and Landsat-8, on the GEE platform [32]. The samples were divided into rapeseed, wheat, trees, shrublands, river, aqua-farm ponds, built-up, greenhouses, and solar panels. These landscapes were split into three groups: rapeseed formed a group; wheat, trees, and shrublands were grouped into other vegetation; and river, aqua-farm ponds, built-up, greenhouses, and solar panels were grouped into non-vegetation. The number of samples is shown in Table 2, and their distribution is shown in Figure 2. Notably, all the samples in Jiangsu Province were only used for validation, while the samples in Xinghua County were split into training and validation samples. The former was used to develop the rapeseed automatic method by analyzing spectral temporal behaviors; the latter was used for validation.

Table 2. The number of different kinds of landcovers.

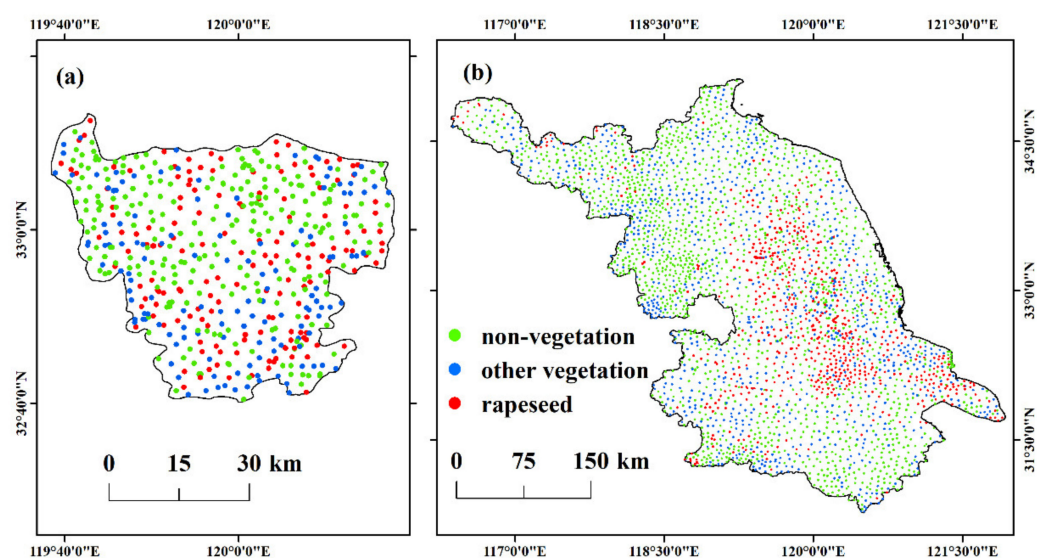| Class	Xinghua County	Jiangsu Province	Total
Non-vegetation	247	1575	1822
Other vegetation	140	860	1000
Rapeseed	163	625	788
Total	550	3060	3610

Figure 2. Location of samples: (**a**) the distribution of training and validation samples in Xinghua County; (**b**) the distribution of validation samples in Jiangsu Province.

2.3. Remote Sensing Data

Remote sensing images were retrieved from the GEE platform. The GEE cloud-computed platform provides large remotely sensed images and vast computing power. Considering the access and the consistency of Sentinel-2, Landsat-7, and Landsat-8, several bands, including red, green, blue, NIR, SWIR1, and SWIR2, of these three sensors were selected [33]. In particular, the B8A band of Sentinel-2 was selected for the NIR band because it is a better match for Landsat imagery [4]. In this study, images taken during the rapeseed growth cycle were used for spectral analysis, and images taken during the rapeseed flowering period were used for rapeseed mapping.

2.4. Data Preprocessing

Images in the GEE platform are well preprocessed with radiometric calibration and registration [16,33]. Thus, the image preparation process included cloud removal, harmonization, and temporal aggregation.

Cloud removal was the first preprocessing step. Jiangsu Province is always cloudy during the rapeseed life cycle. Due to cloud and shadow contamination, it is a challenge to obtain cloud-free images during a specific period [34]. To reduce the effect of clouds, different cloud removal methods were used for different datasets [35]. The Quality Assessment (QA) band was used to identify clouds, and then the mask function was applied to remove pixels whose cloud cover was less than 50% in the Landsat series [16,36,37], while the Sentinel-2 probability dataset was used to detect clouds in Sentinel-2 imagery [38].

The second preprocessing step was harmonization. After cloud removal, there were some missing data in the imagery. Before using temporal aggregation to fill these missing pixels, harmonization needs to be carried out to reduce the differences in resolution, spectral bandwidth, spectral response function, and the field of view of the different sensors because Jiangsu Province is such a cloudy region that it is a challenge to obtain a completely clear image during the rapeseed growing period with standalone sensor imagery. Here, the widely used linear regression was used to reduce the spectral difference between sensors [39–42]. The linear regression formula is shown in Table 3 [42]. ETM+ and OLI imagery were harmonized to the reference of MSI data [40]. Thereafter, these imageries were compiled into one image dataset called the Harmonized Landsat and Sentinel-2 (HLS) dataset [43].

Table 3. The transformation formula from Landsat to Sentinel-2.

Band	ETM+ to MSI	OLI to MSI
Red	MSI = 1.1060 ETM − 0.0139	MSI = 1.0946 OLI − 0.0107
Green	MSI = 0.9909 ETM + 0.0041	MSI = 1.0043 OLI + 0.0026
Blue	MSI = 1.0568 ETM − 0.0024	MSI = 1.0524 OLI − 0.0015
NIR	MSI = 1.0045 ETM − 0.0076	MSI = 0.8954 OLI + 0.0033
SWIR1	MSI = 1.0361 ETM + 0.0041	MSI = 1.0049 OLI + 0.0065
SWIR2	MSI = 1.040 ETM + 0.0086	MSI = 1.0002 OLI + 0.0046

Temporal aggregation was the final preprocessing step. It was carried out using the median algorithm on the GEE platform. As a result, a median value layer stack of every pixel in a time-series image dataset was calculated and used to fill in the missing pixels caused by cloud removal [4,13]. Moreover, the median value layer stack prevented oversaturation and lower values; thus, the time-series data could be smoothed [16,44]. The time window was not the same for every temporal aggregation application. A shorter one may lead to noise; a longer one may cause the loss of critical phenological information. There are options for time intervals for temporal aggregation when performing diverse functions. Here, temporal aggregation was used three times, and each time had a different time window. First, the HLS dataset was daily aggregated to analyze the temporal behaviors of all the selected bands so that the high temporal resolution could keep tracking the entire trajectory of the landscapes. Moreover, daily aggregation allows for the median value

to be calculated in overlapping images for the same day, paving the way for analysis. Second, the time-series Normalized Difference Rapeseed Index (NDRI) and NDVI datasets were monthly aggregated because the monthly temporal curve was enough to capture key information. Third, the flowering phase (from 1 March to 30 May) phenological window was used to produce a seamless cloud-free composite image covering Jiangsu Province. The number of images available is shown in Table 4. All images listed in Table 4 were used in spectral temporal analysis; images taken during March and April were used for rapeseed mapping.

Table 4. Number of images available for each month in Jiangsu Province.

Image Acquisition Period	Number of Sentinel-2 MSI Images	Number of Landsat-8 OLI Images	Number of Landsat-7 ETM+ Images	Total Number of Images
November	129	14	9	152
December	129	17	12	158
January	48	9	6	63
February	81	10	7	98
March	114	16	8	138
April	120	18	14	152
May	118	18	7	143

3. Two-Stepwise Hierarchical Adaptive-Threshold-Based Rapeseed Mapping Model

The two-stepwise hierarchical adaptive-threshold-based method (THAT) was introduced to automatically extract rapeseed in Xinghua County, and it was tested in both Xinghua and Jiangsu. The workflow is shown in Figure 3. First, cloud detection, imagery harmonization, and temporal aggregation were applied to prepare an HLS dataset. Thereafter, the HLS dataset was smoothed using the Savitzky–Golay (S-G) filter, and then it was used to analyze the temporal characteristics of the different bands of the various landcovers. A new vegetation index named the Normalized Difference Rapeseed Index (NDRI) was developed according to the temporal spectral analysis. A two-stage hierarchical classification was proposed to first extract vegetation and then rapeseed [20,45]. Using the NDVI and the Otsu thresholding method (NDVI-Otsu), the non-vegetation landcover was masked because this study focused only on vegetation. Next, NDRI was combined with the adaptive threshold to automatically extract rapeseed. When using NDRI and the Otsu thresholding method, it is called NDRI-Otsu; when using NDRI and the OCED thresholding method, it is called NDRI-OCED. Finally, validation was used to evaluate the potential of the developed method.

3.1. Construction of Normalized Difference Rapeseed Index Using Temporal Spectral Analysis

To select optimal features, temporal spectral analysis was conducted to understand the temporal spectral trajectory of different landcovers during the rapeseed growth cycle [16,26,46]. The spectral reflectance of vegetation is seasonal, expressing phenological details at the different growth stages that can be used to extract certain crops from other crops that share a similar spectrum [7,13]. Before temporal analysis, the S-G filter was adopted to smooth the time-series spectral bands [34]. The optimal bands were selected based on one premise: if there are maximum and minimum bands in a rapeseed field in a certain period, these bands are the optimal bands that can be used to determine the features that distinguish rapeseed from other vegetation [17].

As a further step, the Jeffries–Matusita (JM) distance was calculated to quantitatively compare the indices commonly used in rapeseed mapping [5]. Here, the sample data of trees, shrublands, and wheat were grouped into the other category, and then the JM distance was calculated between the rapeseed (object) and other (background) sample data.
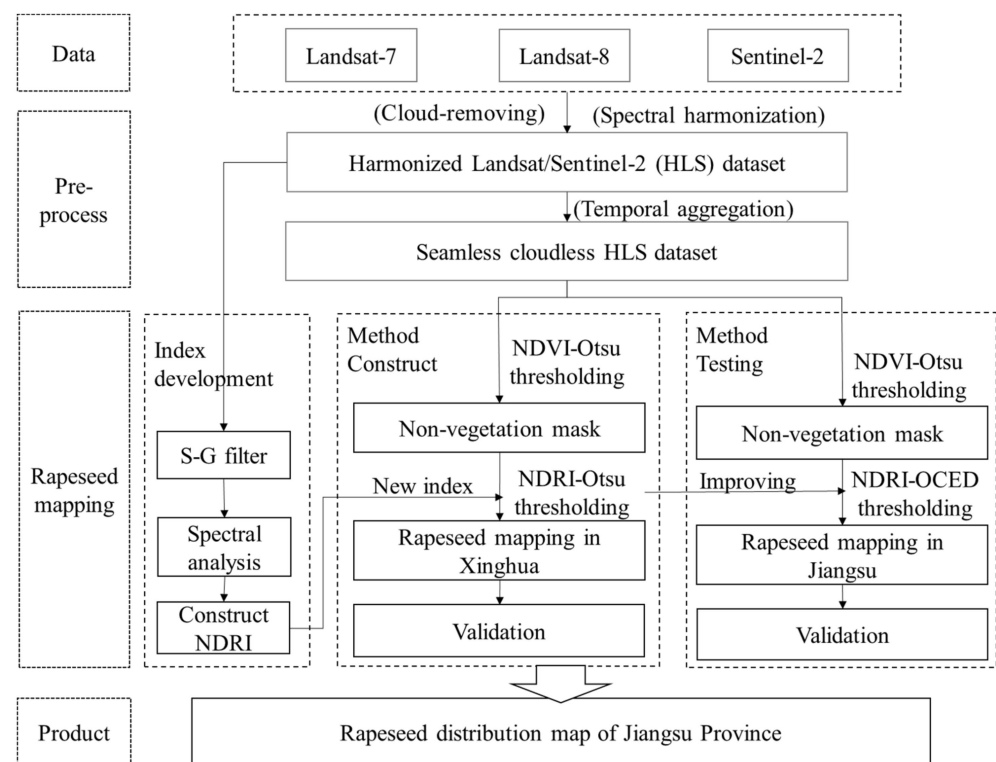
Figure 3. Workflow of two-stepwise hierarchical adaptive thresholding (THAT) rapeseed mapping method.

3.2. NDVI-Otsu Thresholding Method for Non-Vegetation Masking

SWIR is sensitive to water information, including subtle differences in soil moisture and leaf water [27]. To avoid the effects of rivers, lakes, ponds, and weather conditions (such as rain), NDVI was calculated to erase the non-vegetation area, including built-up, river, aqua-farm ponds, panels, and greenhouses, where NDVI was usually lower than vegetation [5,22,47]. The masking threshold was obtained using the Otsu algorithm (see Section 3.3) [23]. The formula of NDVI is described in Equation (1):

$$NDVI = (\rho_{nir} - \rho_{red}) / (\rho_{nir} + \rho_{red}) \tag{1}$$

where ρ_{nir} and ρ_{red} represent the reflectance of the NIR band and red band, respectively.

3.3. Adaptive Thresholding Method to Extract Rapeseed

As mentioned in Section 1, the commonly used empirical threshold method suffers from low applicability. Hence, this study adopted an adaptive thresholding method to overcome the weakness of uniform thresholds. Here, this study introduced two kinds of adaptive thresholding methods and developed a threshold-based rapeseed mapping method. To evaluate the threshold selected using the adaptive thresholding method, the empirical thresholding value was utilized as a comparison. The optimal empirical threshold value was chosen according to the overall accuracy (OA) calculated at every threshold value with steps of 0.01 from -0.30 to -0.10.

The Otsu algorithm is widely used in simple image segmentation where objects and backgrounds have huge differences [48]. It is a threshold selection method solely based on gray-level histograms with no prior knowledge [23]. The interclass variance is iteratively obtained from the histogram of the image for each threshold (see Equation (2)). The maximum interclass variance corresponds to the optimal threshold [22].

$$BSS = \sum_{k=1}^{p} \left(\overline{V}_k - \overline{V} \right)^2 \tag{2}$$

where *BSS* means the between sum-of-squares, describing the interclass variance quantitatively; p represents the number of categories, which is defined as 2 in this study; *V* is the value of the band used for segmentation; and category k is assigned by every *V* less than a specific threshold.

Although the Otsu algorithm provides a changeable threshold value for different environments, it has a limitation in that its accuracy becomes lower when facing a complicated image that contains several categories to classify [23] or the background is much larger than the object pixels [22]. To solve this problem, a combination of the Otsu thresholding method and Canny Edge Detection (OCED) was introduced [20,22]. There was a drastic difference at the boundary between rapeseed and non-rapeseed in NDRI, which could be detected by Canny Edge Detection (CED). It is noteworthy that, after the OCED process, the redundant pixels were cut, leaving the informative boundary pixels preserved. Thus, the histogram distribution represented the boundary of the rapeseed and other vegetation, containing a more balanced proportion of object and background. Thus, the accuracy of the Otsu algorithm improved [20,22].

In conclusion, the THAT automatic rapeseed mapping model can be described as follows:

$$P_{rapeseed} = \left\{ P_i \middle| NDVI_i > T_1 \bigcap NDRI_i > T_2 \right\} \tag{3}$$

where $P_{rapeseed}$ means the pixels considered as rapeseed; P_i means pixel i in the image; and $NDVI_i$ and $NDRI_i$ mean the *NDVI* and *NDRI* values of pixel P_i, respectively. T_1 is the threshold derived from the Otsu thresholding algorithm with the whole *NDVI* image, while T_2 is the threshold derived from the adaptive algorithm (Otsu method or OCED model) with the *NDRI* image masked *NDVI* > T_1.

3.4. Validation to Evaluate the Ability of the THAT Method

The accuracy assessment included two kinds of validation methods. First, samples were used to calculate the confused matrix, OA, user accuracy (UA), producer accuracy (PA), and kappa coefficient [49]. Second, the rapeseed mapping result based on OCED-THAT was compared with that based on the Otsu method, as well as widely used Random Forest classifiers; Random Forest is a stable, efficient, easily parameterized ensemble learning method and fits well in remote sensing classification [50]. Notably, only NDVI and NDRI were used in RF in order to maintain consistency with the THAT method.

4. Results

4.1. Development of New Feature for Rapeseed Extraction

According to the spectral temporal analysis shown in Figure 4, rapeseed achieved the maximum value among all the vegetation in the visible red and green bands during the flowering period, as Davoud (2019) found in their study [9]. In contrast, the SWIR bands achieved the minimum value during the same period. Therefore, rapeseed achieved the maximum and minimum values during the flowering period, which follows the premise mentioned in Section 3.1. The green band was the most striking out of the visible bands, and SWIR1 was the most striking out of the SWIR bands. Accordingly, the green band and the SWIR1 band were selected as the optimal bands to extract rapeseed. The normalized difference between these two bands was computed so that the result could be confined to the range [−1, 1] [28,51]. In this way, the Normalized Difference Rapeseed Index (NDRI) [21] was developed. The formula of NDRI is described in Equation (4):

$$NDRI = (\rho_{green} - \rho_{swir1}) / (\rho_{green} + \rho_{swir1}) \tag{4}$$

where ρ_{green} and ρ_{swir1} represent the reflectance of the green band and the SWIR1 band, respectively.
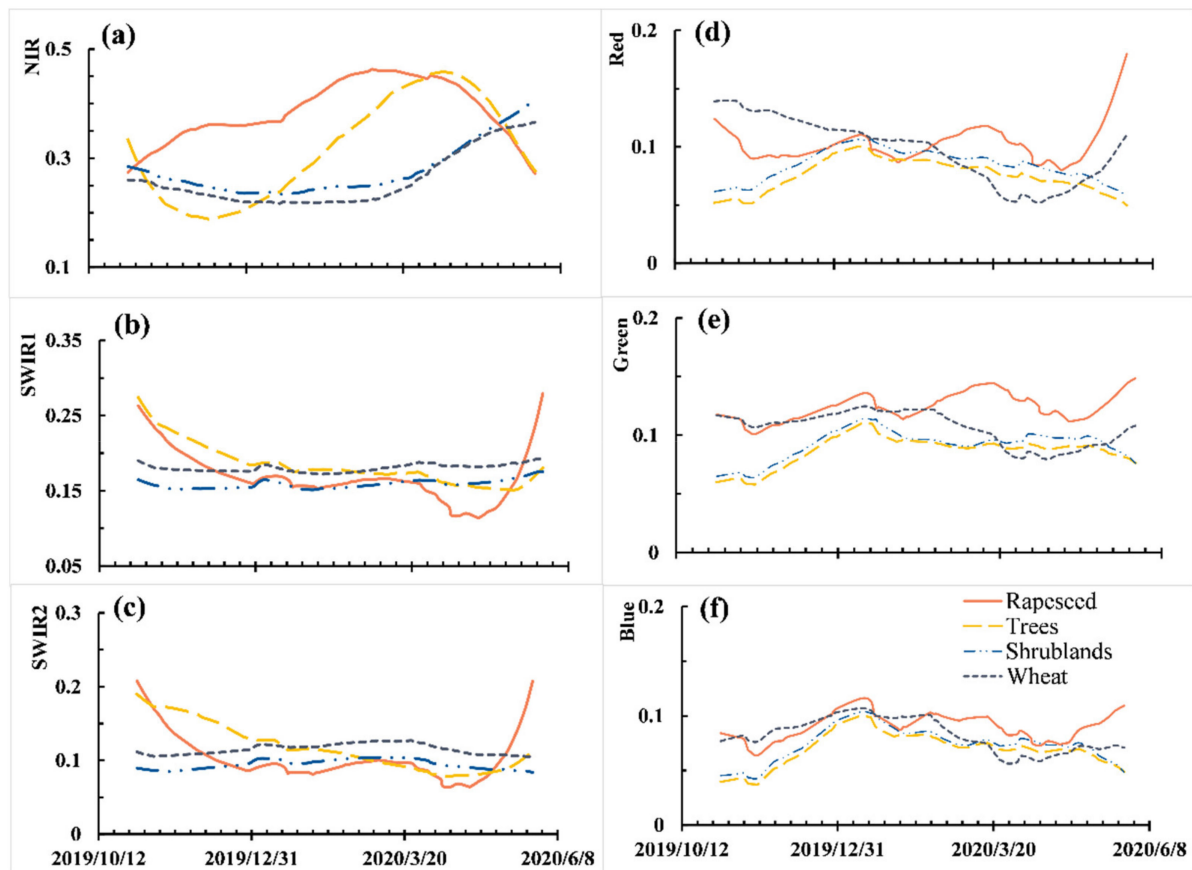
Figure 4. Temporal spectral profile of different landcovers at (**a**) near-infrared, (**b**) short-wave infrared 1, (**c**) short-wave infrared 2, (**d**) red, (**e**) green, and (**f**) blue wavebands.

Figure 5 exhibits the temporal trajectory of several commonly used vegetation indices for rapeseed extraction. In the NDRI temporal profile shown in Figure 5a, a separation gap between rapeseed and other vegetation was found during the flowering period. The mean NDRI value of rapeseed was about −0.1, while the mean values of other vegetation were clustered around −0.35, theoretically forming a histogram with a bimodal pattern that can be segmented using the thresholding algorithm. Concerning the NDYI displayed in Figure 5c, the mean NDYI value of rapeseed was about 0.25 while that of wheat was around 0.2, and the other had a mean value of 0.12; therefore, a theoretical three-peaked histogram can be generated, which is challenge to segment with one single threshold. As for the NDVI and RRCI values illustrated in Figure 5b,d, thresholding segmentation was not an ideal method to extract rapeseed from these features.

As Table 5 illustrates, the JM distance indicates that NDRI outperformed other vegetation indices, including NDVI, NDYI, and RRCI, in rapeseed identification.

Table 5. JM distance between rapeseed and other vegetation in different vegetation index.

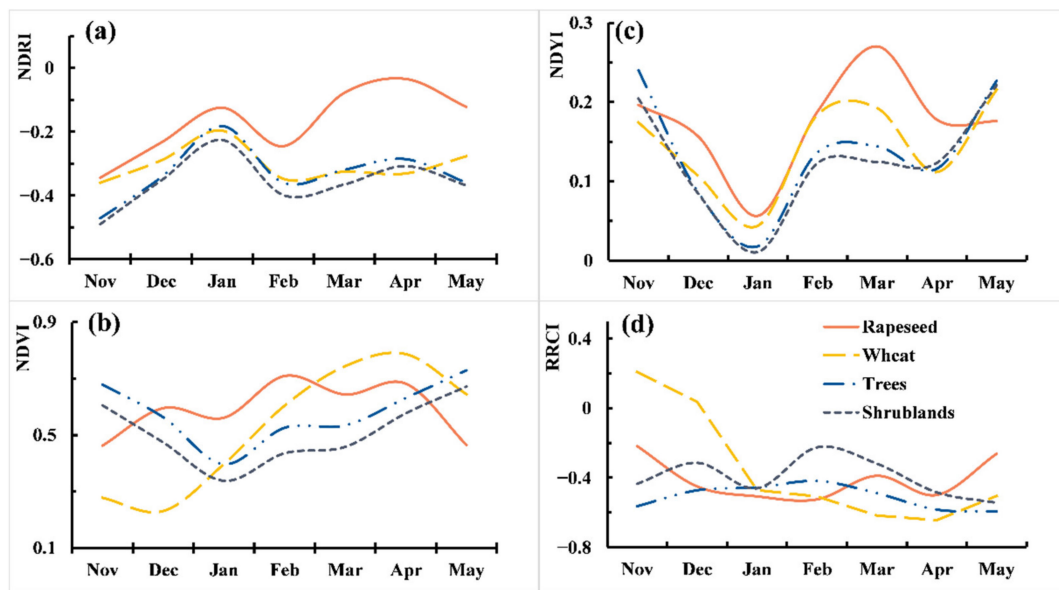| Index	JM Distance Value
NDVI	0.5904
NDYI	0.5487
NDRI	1.0425
RRCI	0.7464

Figure 5. Temporal profile of different vegetation with the (**a**) Normalized Difference Rapeseed Index (NDRI), (**b**) Normalized Difference Vegetation Index (NDVI), (**c**) Normalized Difference Yellow Index (NDYI), and (**d**) Ratio Oilseed Rape Colorimetric Index (RRCI).

4.2. Threshold Selection for Rapeseed Extraction

For the non-vegetation mask, the NDVI threshold values were 0.4456 in Xinghua County and 0.3671 in Jiangsu Province.

For the extraction of rapeseed, the NDRI threshold values are displayed in Figure 6. In Xinghua County, the threshold values were −0.2267 and −0.1485 corresponding to the Otsu and OCED thresholding algorithms, respectively, as shown as Figure 6a,b. In Jiangsu Province, the threshold values were −0.2893 and −0.1648 corresponding to the Otsu and OCED thresholding methods, respectively, as shown as Figure 6c,d. As seen in Figure 7, the threshold value of −0.13 was the appropriate empirical threshold corresponding to the peak accuracy in Xinghua County. Conversely, this value was not appropriate in Jiangsu Province. The threshold calculated using the OCED algorithm outperformed the empirical threshold and the Otsu threshold.
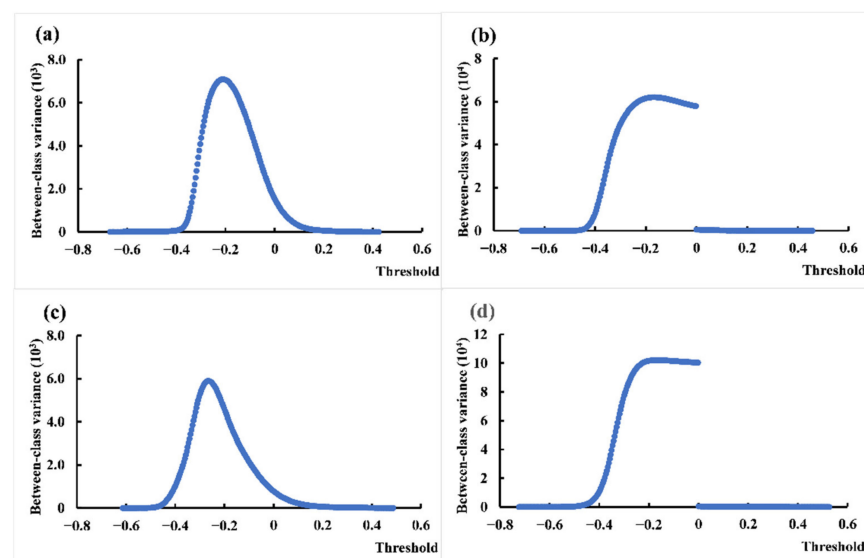

Figure 6. Comparison of thresholding selection. The peak between-class variance corresponds to the optimal threshold value. Panels (**a**,**c**) are Otsu-based thresholds selected in training area and testing

area, respectively. Panels (**b**,**d**) are OCED-based (Otsu with Canny Edge Detection) thresholds selected in training area and testing area, respectively.
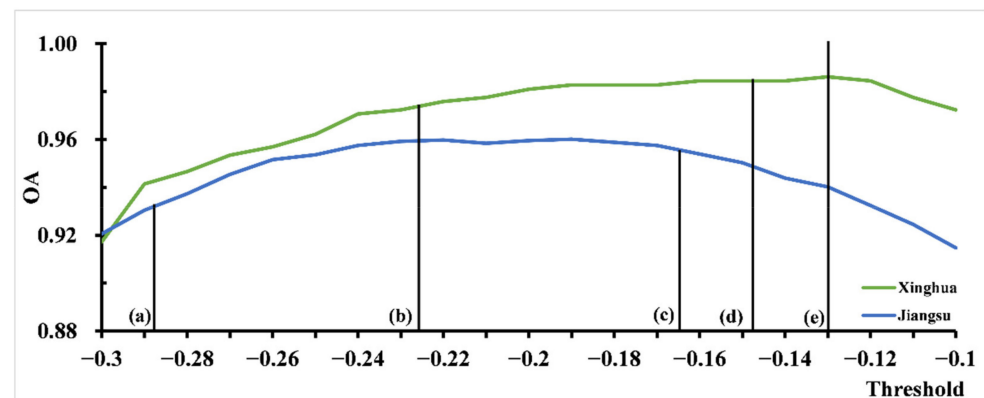

Figure 7. Empirical threshold in Xinghua County and Jiangsu Province. The green and blue curves are overall accuracy (OA) values at every empirical threshold in Xinghua and Jiangsu, respectively. Panel (**a**) is the threshold selected using Otsu method in Jiangsu Province; panel (**b**) is the threshold selected using Otsu method in Xinghua County; panel (**c**) is the threshold selected using Otsu with Canny Edge Detection (OCED) method in Jiangsu Province; panel (**d**) is the threshold selected using OCED method in Xinghua County; and panel (**e**) is the empirical threshold value determined in Xinghua while applied in Jiangsu.

4.3. Accuracy Assessment and Comparison

Figure 8 depicts the overall extent of rapeseed distribution in both Xinghua and Jiangsu in 2020 using three methods. Figure 9 displays zoom-in view of sites A and B in Figure 8. In the optical true-color composite images of sites A and B displayed in Figure 9(1), rapeseed was yellow-green, and the other crops are dark green. By zooming in on three case regions of sites A and B (Figure 9a,c), it was found that the results of the OCED (demonstrated in Figure 9(2)) and Random Forest (shown in Figure 9(4)) had a high spatial consistency with the true-color optical Sentinel-2 image (Figure 9(1)), while the result of the Otsu suffered from noticeable errors as displayed in Figure 9(3). As Figure 6 shows, the NDRI threshold based on the Otsu was lower than that based on the OCED method. Conversely, as depicted in Figure 5a, rapeseed achieved a higher NDRI value than other vegetation. Therefore, a lower threshold derived from the Otsu method would lead to more commission errors.

Table 6 illustrates that the Otsu-based rapeseed map in Xinghua County in 2020 (Figure 8) had a high accuracy with the OA and kappa coefficient in the order of 0.9724 and 0.9327, respectively. However, when this method was used in Jiangsu Province, where the environment is larger and more complicated, the OA and kappa coefficient decreased to 0.9310 and 0.8089, respectively. The kappa coefficient was slightly improved in Xinghua County and remarkably increased in Jiangsu Province based on the OCED thresholding algorithm. Compared with the RF-based method, the kappa coefficient of the THAT-based method was close to that in Xinghua County while slightly lower than that in Jiangsu Province. A comparison between the RF-based and the OCED-based rapeseed maps showed that the spatial distribution of these two products (Figure 9) had a high consistency in Jiangsu Province. The OCED-based method was more likely to cause underestimation but at an acceptable level. This suggests the potential of the OCED-based method to extract rapeseed from other vegetation with optically sensed images.
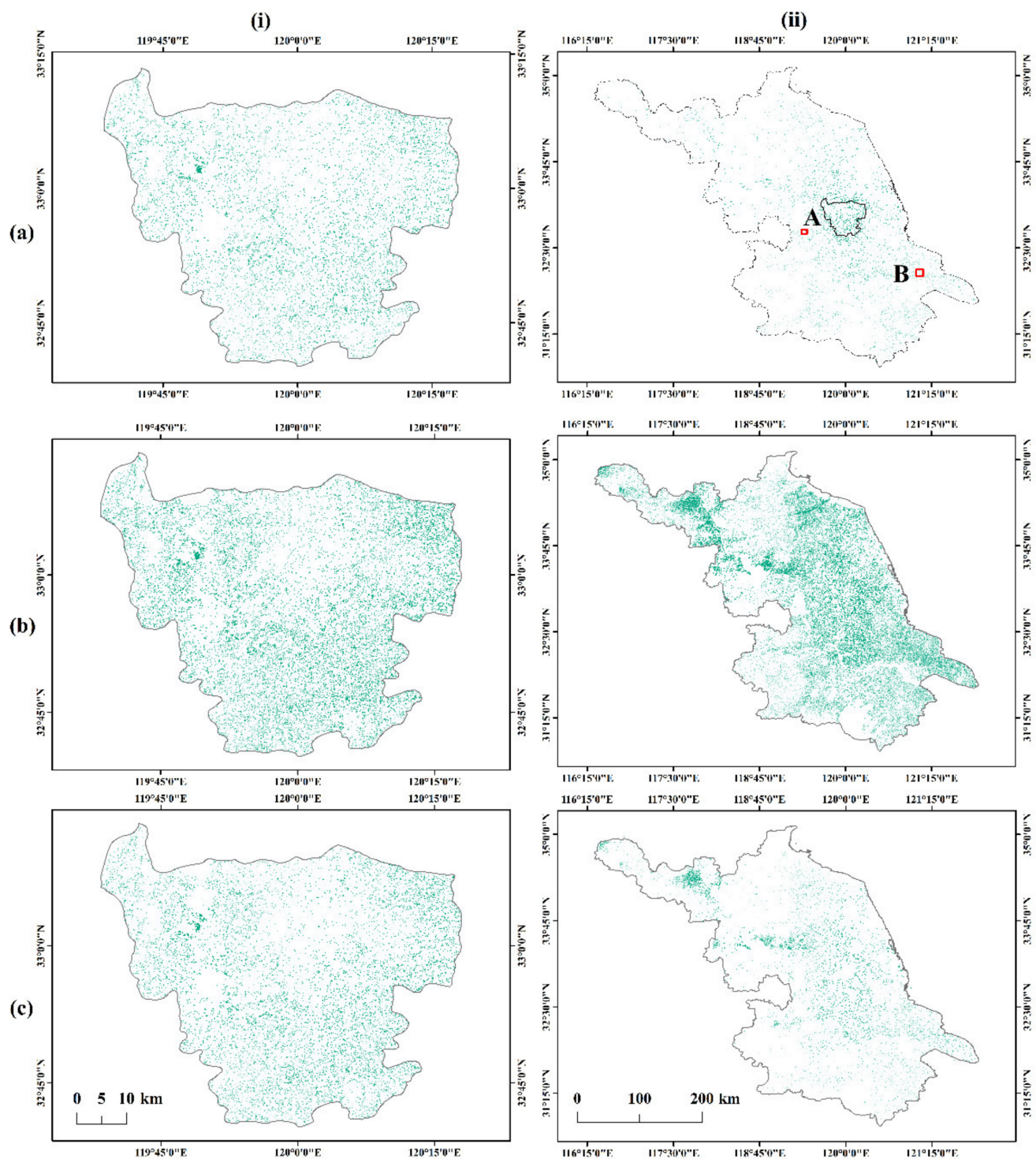
Figure 8. The overall view of rapeseed maps in (**i**) training area, Xinghua County, and (**ii**) testing area, Jiangsu Province, in 2020. Panels (**a**–**c**) are the rapeseed maps derived from OCED-THAT method, Otsu-THAT method, and RF classification method, respectively. Here, OCED means Otsu with Canny Edge Detection thresholding algorithm, and THAT means two-stepwise hierarchical adaptive thresholding method.

Figure 9. The zoom-in view of (**a**) site A, (**b**) the red box of site A, (**c**) site B, and (**d**) the red box of site B. Row (1) shows the pseudo-true-color composite image of positions (**a**–**d**). Rows (2–4) display the OCED-THAT-based, Otsu-THAT-based, and Random Forest-based rapeseed maps corresponding to places in row (1). Here, OCED means Otsu with Canny Edge Detection thresholding algorithm, and THAT means two-stepwise hierarchical adaptive thresholding method.
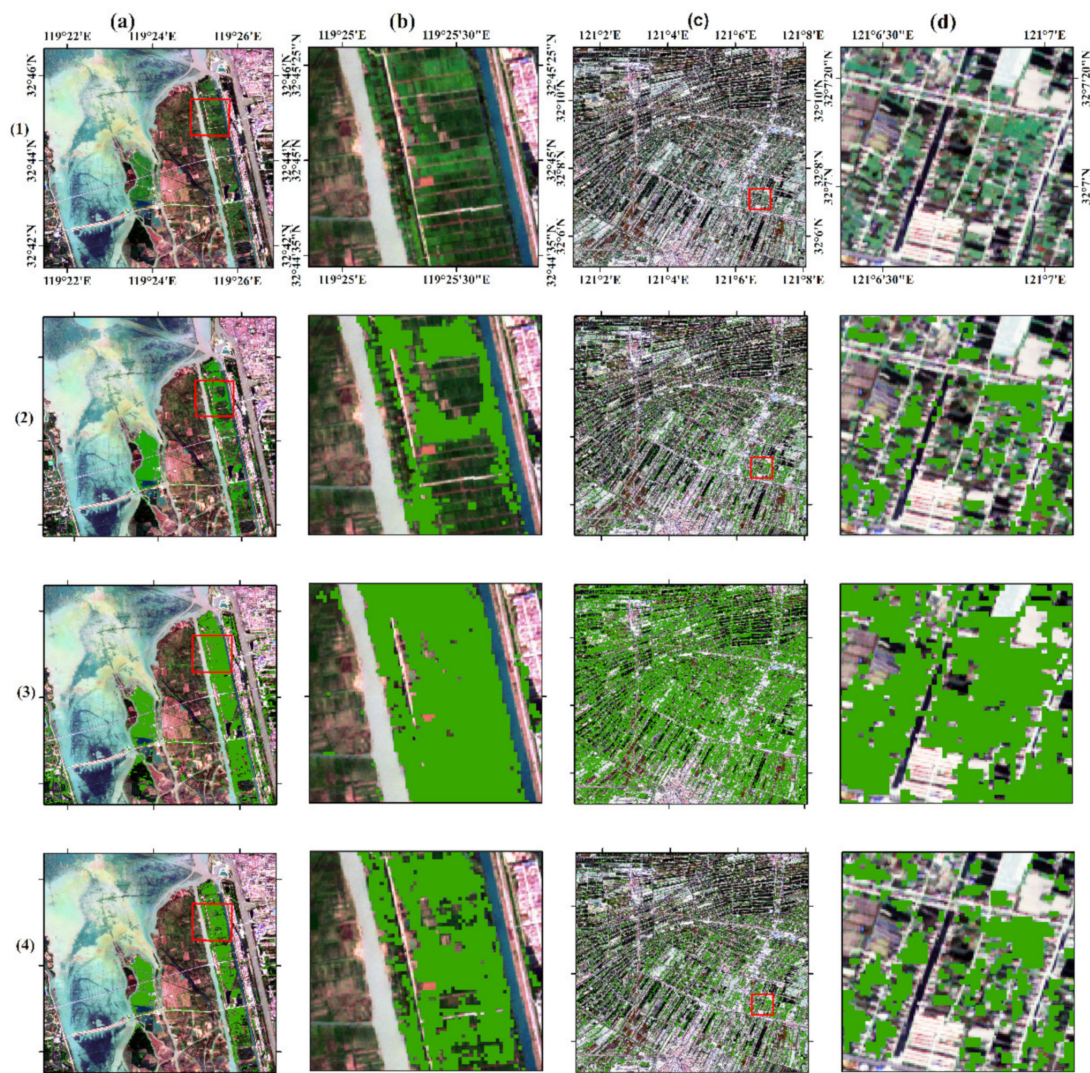
Table 6. Accuracy of different rapeseed mapping methods.

Region	Thresholding Method	OA	Kappa	PA	UA
Xinghua County	Otsu	0.9724	0.9327	0.9298	0.9755
	OCED	0.9845	0.9614	0.9813	0.9632
	RF	0.9840	0.9603	0.9917	0.9520
Jiangsu Province	Otsu	0.9310	0.8089	0.7556	0.9792
	OCED	0.9559	0.8569	0.9554	0.8224
	RF	0.9806	0.9391	0.9527	0.9497

5. Discussion

Several factors influence the accuracy of classification, namely, separability in spectral features between objects and backgrounds, the optimum threshold, and the availability of cloudless datasets [45].

5.1. The Potential of NDRI in Rapeseed Mapping

This study verified the potential of the NDRI vegetation index for rapeseed discrimination. The fact that rapeseed undergoes two obvious changes during the flowering stage provides theory support for the application of NDRI to identify rapeseed. Firstly, blooming makes the reflectance of the rapeseed field turn from foliar information to a mixture of foliar and floral signals [1]. Therefore, the intensity of the green band increases corresponding to the yellow-green blossom, since the yellow color is a mixture of green and red rays [1]. Secondly, during the reproductive stage, rapeseed needs more water, and evapotranspiration also increases [52,53]. As a result, the spectral reflection of the rapeseed field contains changes in water content. The SWIR1 band of rapeseed shows a significant reduction during the flowering stage, correlating to the increase in evapotranspiration, whereas other vegetation remains stable. Not only does NDRI show a huge separation between rapeseed and other vegetation, but it also keeps the value of rapeseed at its highest among all the vegetation. Thus, rapeseed and other vegetation form a bimodal image, which provides a means to apply the adaptive thresholding algorithm in crop mapping. It is noteworthy that Xu (2006) developed the Modified Normalized Difference Water Index (MNDWI) for water extraction, as it shared exactly the same band composite with NDRI [21].

However, the red-edge wavelength was not considered in this study because Landsat imagery does not contain red-edge waveband information, making harmonization with Sentinel-2 imagery challenging. Future studies may focus on the difference in red-edge information between rapeseed and other vegetation [8]. In addition to spectral features, the application of point clouds and plant height features [54] could also be considered in the future.

5.2. Adaptive Threshold Method in Crop Mapping

In this paper, the adaptive thresholding method was used to select an optimal NDVI threshold for non-vegetation masking and an optimal NDRI threshold for rapeseed extraction. The adaptive threshold method is widely used in algae monitoring since the spectral difference between water bodies and algae is very large. In contrast, there is a significant lack of adaptive threshold applications in crop mapping because the histograms of vegetation with the most commonly used indices are multimodal, which decreases the accuracy of the adaptive thresholding method [20,22,23]. Consequently, the threshold is usually empirically selected in previous studies [17,55], which affects the accuracy of the crop map products [7,44]. The results of our study indicate that the OCED method had good performance, with an OA of 0.9559 and a kappa of 0.8569.

However, we can envision more challenges when our method is replicated in large regional studies. Since GEE often needs zoning processing due to the user's memory limitations, some pseudo-rapeseed pixels will still be extracted when using the OCED method in the case of large-scale zoning processing if the rapeseed is not well distributed and there happens to be no rapeseed in some sub-regions. Thus, improvements should be made to detect whether there is any rapeseed. Only if there are any rapeseed pixels existing can the automatic rapeseed mapping algorithm operate.

5.3. Solution for Cloudy Regions

In this research, multi-sensor temporal aggregation was applied to improve temporal resolution in order to reduce cloud contamination. In the southern region of China, it is often cloudy and rainy, and optical remote sensing images are susceptible to cloud contamination, causing a reduction in the number of available images [13,22,56]. Additionally, temporal resolution is more critical for crop extraction because an insufficient temporal resolution can easily lose the information of crucial crop growth periods [55]. In particular, NDRI contains the SWIR band, which is sensitive to clouds. Accordingly, the influence of clouds should be considered [57]. High spatial and temporal resolution satellite datasets may be a good solution to reduce the influence of clouds [7]. Thus, in this study, Landsat 7, Landsat 8, and Sentinel 2 images were compiled into one dataset to improve the number of

good-quality observations during the flowering period to obtain higher accuracy rapeseed mapping in a cloudy region.

As a cash crop, rapeseed is cultivated in patches in southern China, leading to a spectral mixture in remote sensing images [17]. Furthermore, rapeseed mapping requires a high spatial resolution image, which is in contrast to the mapping of bulk crops (e.g., wheat and paddy rice). However, the HLS image had a coarser spatial resolution (30 m) than the standalone Sentinel-2 image (10 m). Recently, the application of deep learning was considered in a study to extract rapeseed in cloudy regions, and it attained a satisfactory result [5]. Future research may focus on combining the deep learning technique and the threshold method [5]. In addition to optical remote sensing, combinations with radar data are expected to improve the accuracy of crop extraction in cloudy and rainy areas [8,13,26,43,56,58].

6. Conclusions

This study developed a new index for rapeseed identification called the Normalized Difference Rapeseed Index (NDRI) by analyzing the temporal profile of wavebands. The Jeffries–Matusita (JM) distance was utilized to evaluate the separability of rapeseed and other vegetation, and it was found that NDRI outperformed NDVI, NDYI, and RRCI in rapeseed mapping. Moreover, adaptive thresholding methods, including Otsu and Otsu with Canny Edge Detection (OCED), were conducted to choose an optimum threshold value. When comparing these methods, the OCED proved to be the best among the Otsu and empirical threshold methods. Based on NDRI and the adaptive thresholding method, a two-stepwise hierarchical adaptive thresholding method for rapeseed discrimination was developed in Xinghua County and extended to Jiangsu Province, China. The proposed method had a satisfying accuracy without training data, keeping a high consistency with pseudo-true-color composite images. In future research, more classification features should be fully utilized, such as red-edge features.

Author Contributions: Conceptualization, S.C. and Z.L.; methodology, S.C.; software, S.C.; validation, T.J., X.G., and Z.L.; formal analysis, S.C.; investigation, X.J.; resources, X.J., J.P., Z.L. and H.Z.; data curation, T.J.; writing—original draft preparation, S.C.; writing—review and editing, Z.L. and W.Z.; visualization, S.C.; supervision, Z.L.; project administration, J.P.; funding acquisition, Z.L and S.C. All authors have read and agreed to the published version of the manuscript.

Data Availability Statement: Not applicable.

Conflicts of Interest: The authors declare no conflict of interest.

References

1. Sulik, J.J.; Long, D.S. Spectral considerations for modeling yield of canola. *Remote Sens. Environ.* **2016**, *184*, 161–174. [CrossRef]
2. Tao, J.; Wu, W.; Liu, W.; Xu, M. Exploring the Spatio-Temporal Dynamics of Winter Rape on the Middle Reaches of Yangtze River Valley Using Time-Series MODIS Data. *Sustainability* **2020**, *12*, 20466. [CrossRef]
3. Pan, Z.; Huang, J.; Wang, F. Multi range spectral feature fitting for hyperspectral imagery in extracting oilseed rape planting area. *Int. J. Appl. Earth Obs. Geoinf.* **2013**, *25*, 21–29. [CrossRef]
4. Jun, X.; Prasad, T.; James, T.; Murali, G.; Pardhasaradhi, T.; Adam, O.; Russell, C.; Kamini, Y.; Noel, G. Nominal 30-m Cropland Extent Map of Continental Africa by Integrating Pixel-Based and Object-Based Algorithms Using Sentinel-2 and Landsat-8 Data on Google Earth Engine. *Remote Sens.* **2017**, *9*, 1065. [CrossRef]
5. Zhang, H.; Liu, W.; Zhang, L. Seamless and automated rapeseed mapping for large cloudy regions using time-series optical satellite imagery. *ISPRS J. Photogramm. Remote Sens.* **2022**, *184*, 45–62. [CrossRef]
6. Adrian, J.; Sagan, V.; Maimaitijiang, M. Sentinel SAR-optical fusion for crop type mapping using deep learning and Google Earth Engine. *ISPRS J. Photogramm. Remote Sens.* **2021**, *175*, 215–235. [CrossRef]

7. Liu, J.; Feng, Q.; Gong, J.; Zhou, J.; Liang, J.; Li, Y. Winter wheat mapping using a random forest classifier combined with multi-temporal and multi-sensor data. *Int. J. Digit. Earth* **2018**, *11*, 1–20. [CrossRef]

8. He, Y.; Dong, J.; Liao, X.; Sun, L.; Fu, P. Examining rice distribution and cropping intensity in a mixed single- and double-cropping region in South China using all available Sentinel 1/2 images. *Int. J. Appl. Earth Obs. Geoinf.* **2021**, *101*, 102351. [CrossRef]

9. Ashourloo, D.; Shahrabi, H.S.; Azadbakht, M.; Aghighi, H.; Nematollahi, H.; Alimohammadi, A.; Matkan, A.A. Automatic canola mapping using time series of sentinel 2 images. *ISPRS J. Photogramm. Remote Sens.* **2019**, *156*, 63–76. [CrossRef]

10. D'Andrimont, R.; Taymans, M.; Lemoine, G.; Ceglar, A.; Velde, M. Detecting flowering phenology in oil seed rape parcels with Sentinel-1 and -2 time series. *Remote Sens. Environ.* **2020**, *239*, 111660. [CrossRef]

11. Meng, S.; Zhong, Y.; Luo, C.; Hu, X.; Huang, S. Optimal Temporal Window Selection for Winter Wheat and Rapeseed Mapping with Sentinel-2 Images: A Case Study of Zhongxiang in China. *Remote Sens.* **2020**, *12*, 226. [CrossRef]

12. Inglada, J.; Vincent, A.; Arias, M.; Marais-Sicre, C. Improved Early Crop Type Identification By Joint Use of High Temporal Resolution SAR And Optical Image Time Series. *Remote Sens.* **2016**, *8*, 362. [CrossRef]

13. Griffiths, P.; Nendel, C.; Hostert, P. Intra-annual reflectance composites from Sentinel-2 and Landsat for national-scale crop and land cover mapping. *Remote Sens. Environ.* **2019**, *220*, 135–151. [CrossRef]

14. Kussul, N.; Lavreniuk, M.; Skakun, S.; Shelestov, A. Deep Learning Classification of Land Cover and Crop Types Using Remote Sensing Data. *IEEE Geosci. Remote Sens. Lett.* **2017**, *14*, 778–782. [CrossRef]

15. Wang, D.; Fang, S.; Yang, Z.; Wang, L.; Tang, W.; Li, Y.; Tong, C. A Regional Mapping Method for Oilseed Rape Based on HSV Transformation and Spectral Features. *ISPRS Int. J. Geo-Inf.* **2018**, *7*, 224. [CrossRef]

16. Venkatappa, M.; Sasaki, N.; Shrestha, R.P.; Tripathi, N.K.; Ma, H.-O. Determination of Vegetation Thresholds for Assessing Land Use and Land Use Changes in Cambodia using the Google Earth Engine Cloud-Computing Platform. *Remote Sens.* **2019**, *11*, 1514. [CrossRef]

17. Ashourloo, D.; Shahrabi, H.S.; Azadbakht, M.; Rad, A.M.; Aghighi, H.; Radiom, S. A novel method for automatic potato mapping using time series of Sentinel-2 images. *Comput. Electron. Agric.* **2020**, *175*, 105583. [CrossRef]

18. Ashourloo, D.; Shahrabi, H.S.; Azadbakht, M.; Aghighi, H.; Radiom, S. A Novel Automatic Method for Alfalfa Mapping Using Time Series of Landsat-8 OLI Data. *IEEE J. Sel. Top. Appl. Earth Obs. Remote Sens.* **2018**, *11*, 4478–4487. [CrossRef]

19. Huang, Y.; Qiu, B.; Chen, C.; Zhu, X.; Wu, W.; Jiang, F.; Lin, D.; Peng, Y. Automated soybean mapping based on canopy water content and chlorophyll content using Sentinel-2 images. *Int. J. Appl. Earth Obs. Geoinf.* **2022**, *109*, 102801. [CrossRef]

20. Geethen, S.; Chevonne, R.; Marcus, B.; Benjamin, R. A Remote Sensing Method to Monitor Water, Aquatic Vegetation, and Invasive Water Hyacinth at National Extents. *Remote Sens.* **2020**, *12*, 4021. [CrossRef]

21. Xu, H. Modification of normalised difference water index (NDWI) to enhance open water features in remotely sensed imagery. *Int. J. Remote Sens.* **2006**, *27*, 3025–3033. [CrossRef]

22. Zhang, G.; Wu, M.; Wei, J.; Yufang, H. Adaptive Threshold Model in Google Earth Engine: A Case Study of Ulva prolifera Extraction in the South Yellow Sea, China. *Remote Sens.* **2021**, *13*, 3240. [CrossRef]

23. Otsu, N. A Threshold Selection Method from Gray-Level Histograms. *IEEE Trans. Syst. Man Cybern.* **1979**, *9*, 62–66. [CrossRef]

24. Da Silva, C.A., Jr.; Leonel-Junior, A.H.S.; Rossi, F.S.; Correia Filho, W.L.F.; de Barros Santiago, D.; de Oliveira-Júnior, J.F.; Teodoro, P.E.; Lima, M.; Capristo-Silva, G.F. Mapping soybean planting area in midwest Brazil with remotely sensed images and phenology-based algorithm using the Google Earth Engine platform. *Comput. Electron. Agric.* **2020**, *169*, 105194. [CrossRef]

25. Huete, A.R. A soil-adjusted vegetation index (SAVI). *Remote Sens. Environ.* **1988**, *25*, 295–309. [CrossRef]

26. Veloso, A.; Mermoz, S.; Bouvet, A.; Le Toan, T.; Planells, M.; Dejoux, J.F.; Ceschia, E. Understanding the temporal behavior of crops using Sentinel-1 and Sentinel-2-like data for agricultural applications. *Remote Sens. Environ.* **2017**, *199*, 415–426. [CrossRef]

27. Thenkabail, P.S.; Enclona, E.A.; Ashton, M.S.; Meer, B. Accuracy assessments of hyperspectral waveband performance for vegetation analysis applications. *Remote Sens. Environ.* **2004**, *91*, 354–376. [CrossRef]

28. Gao, B. NDWI-a normalized difference water index for remote sensing of vegetation liquid water from space. *Remote Sens. Environ.* **1996**, *58*, 257–266. [CrossRef]

29. Fu, Y.; Zhou, T.; Yao, Y.; Qiu, A.; Wei, F.; Liu, J.; Liu, T. Evaluating efficiency and order of urban land use structure: An empirical study of cities in Jiangsu, China. *J. Clean. Prod.* **2021**, *283*, 124638. [CrossRef]

30. Yusheng, K.; Ntarmah, A.H. Developing a rural ecological assessment index for Jiangsu Province, China. *J. Nat. Conserv.* **2021**, *64*, 126093. [CrossRef]

31. Yang, L.; Shen, F.; Zhang, L.; Cai, Y.; Yi, F.; Zhou, C. Quantifying influences of natural and anthropogenic factors on vegetation changes using structural equation modeling: A case study in Jiangsu Province, China. *J. Clean. Prod.* **2021**, *280*, 124330. [CrossRef]

32. Venkatappa, M.; Sasaki, N.; Anantsuksomsri, S.; Smith, B. Applications of the Google Earth Engine and Phenology-Based Threshold Classification Method for Mapping Forest Cover and Carbon Stock Changes in Siem Reap Province, Cambodia. *Remote Sens.* **2020**, *12*, 3110. [CrossRef]

33. Gorelick, N.; Hancher, M.; Dixon, M.; Ilyushchenko, S.; Moore, R. Google Earth Engine: Planetary-scale geospatial analysis for everyone. *Remote Sens. Environ.* **2017**, *202*, 18–27. [CrossRef]

34. Liu, L.; Xiao, X.; Qin, Y.; Wang, J.; Qiao, Z. Mapping cropping intensity in China using time series Landsat and Sentinel-2 images and Google Earth Engine. *Remote Sens. Environ.* **2020**, *239*, 111624. [CrossRef]

35. Xu, F.; Li, Z.; Zhang, S.; Huang, N.; Quan, Z.; Zhang, W.; Liu, X.; Jiang, X.; Pan, J.; Prishchepov, A.V. Mapping Winter Wheat with Combinations of Temporally Aggregated Sentinel-2 and Landsat-8 Data in Shandong Province, China. *Remote Sens.* **2020**, *12*, 2065. [CrossRef]

36. Qiu, S.; Zhu, Z.; He, B. Fmask 4.0: Improved cloud and cloud shadow detection in Landsats 4–8 and Sentinel-2 imagery. *Remote Sens. Environ.* **2019**, *231*, 111205. [CrossRef]

37. Foga, S.; Scaramuzza, P.L.; Guo, S.; Zhu, Z.; Dilley, R.D.; Beckmann, T.; Schmidt, G.L.; Dwyer, J.L.; Joseph Hughes, M.; Laue, B. Cloud detection algorithm comparison and validation for operational Landsat data products. *Remote Sens. Environ.* **2017**, *194*, 379–390. [CrossRef]

38. Braaten, J. Sentinel-2 Cloud Masking with s2cloudless. Available online: https://developers.google.com/earth-engine/tutorials/community/sentinel-2-s2cloudless?hl=en (accessed on 8 December 2021).

39. Claverie, M.; Ju, J.; Masek, J.G.; Dungan, J.L.; Vermote, E.F.; Roger, J.C.; Skakun, S.V.; Justice, C. The Harmonized Landsat and Sentinel-2 surface reflectance data set. *Remote Sens. Environ.* **2018**, *219*, 145–161. [CrossRef]

40. Shang, R.; Zhu, Z. Harmonizing Landsat 8 and Sentinel-2: A time-series-based reflectance adjustment approach. *Remote Sens. Environ.* **2019**, *235*, 111439. [CrossRef]

41. Claverie, M.; Masek, J.G.; Ju, J. Harmonized Landsat-8 Sentinel-2 (HLS) Product User's Guide. Available online: https://hls.gsfc.nasa.gov/wp-content/uploads/2017/02/HLS.v1.2.UserGuide.pdf (accessed on 23 December 2021).

42. Rc, A.; Ih, A.; Jg, A.; Mf, A.; Kt, B. Empirical cross sensor comparison of Sentinel-2A and 2B MSI, Landsat-8 OLI, and Landsat-7 ETM+ top of atmosphere spectral characteristics over the conterminous United States. *Remote Sens. Environ.* **2019**, *221*, 274–285. [CrossRef]

43. Ajadi, A.O.; Jeremiah, B.; Sang-Zi, L.; Rogerio, F.; Kumpatla, S.P.; Rinkal, P.; Anu, S. Large-scale crop type and crop area mapping across Brazil using synthetic aperture radar and optical imagery. *Int. J. Appl. Earth Obs. Geoinf.* **2021**, *97*, 102294. [CrossRef]

44. Zhang, W.; Brandt, M.; Prishchepov, A.V.; Li, Z.; Lyu, C.; Fensholt, R. Mapping the Dynamics of Winter Wheat in the North China Plain from Dense Landsat Time Series (1999 to 2019). *Remote Sens.* **2021**, *13*, 1170. [CrossRef]

45. Jain, M.; Mondal, P.; Defries, R.S.; Small, C.; Galford, G.L. Mapping cropping intensity of smallholder farms: A comparison of methods using multiple sensors. *Remote Sens. Environ.* **2013**, *134*, 210–223. [CrossRef]

46. Wu, M.; Huang, W.; Niu, Z.; Wang, Y.; Wang, C.; Li, W.; Hao, P.; Yu, B. Fine crop mapping by combining high spectral and high spatial resolution remote sensing data in complex heterogeneous areas. *Comput. Electron. Agric.* **2017**, *139*, 1–9. [CrossRef]

47. Rouse, J.W., Jr.; Haas, R.H.; Schell, J.A.; Deering, D.W. Monitoring vegetation systems in the greant plains with ERTS. In Proceedings of the Earth Resources Technology Satellite Symposium NASA, Washington, DC, USA, 10–14 December 1973; NASA: Washington, DC, USA, 1973; pp. 309–317.

48. Bai, X.D.; Cao, Z.G.; Wang, Y.; Yu, Z.H.; Zhang, X.F.; Li, C.N. Crop segmentation from images by morphology modeling in the CIE L* a* b* color space. *Comput. Electron. Agric.* **2013**, *99*, 21–34. [CrossRef]

49. Congalton, R.G. A review of assessing the accuracy of classifications of remotely sensed data. *Remote Sens. Environ.* **1991**, *37*, 35–46. [CrossRef]

50. Pelletier, C.; Valero, S.; Inglada, J.; Champion, N.; Dedieu, G. Assessing the robustness of Random Forests to map land cover with high resolution satellite image time series over large areas. *Remote Sens. Environ.* **2016**, *187*, 156–168. [CrossRef]

51. Mcfeeters, S.K. The use of the Normalized Difference Water Index (NDWI) in the delineation of open water features. *Int. J. Remote Sens.* **1996**, *17*, 1425–1432. [CrossRef]

52. Wagle, P.; Gowda, P.H.; Northup, B.K.; Neel, J.P.S. Ecosystem-level water use efficiency and evapotranspiration partitioning in conventional till and no-till rainfed canola. *Agric. Water Manag.* **2021**, *250*, 106825. [CrossRef]

53. Katuwal, K.B.; Cho, Y.; Singh, S.; Angadi, S.V.; Begna, S.; Stamm, M. Soil water extraction pattern and water use efficiency of spring canola under growth-stage-based irrigation management. *Agric. Water Manag.* **2020**, *239*, 106232. [CrossRef]

54. Zhang, P.; Hu, S.; Li, W.; Zhang, C. Parcel-level mapping of crops in a smallholder agricultural area: A case of central China using single-temporal VHSR imagery. *Comput. Electron. Agric.* **2020**, *175*, 105581. [CrossRef]

55. Dong, J.; Xiao, X.; Menarguez, M.A.; Zhang, G.; Qin, Y.; Thau, D.; Biradar, C.; Moore, B. Mapping paddy rice planting area in northeastern Asia with Landsat 8 images, phenology-based algorithm and Google Earth Engine. *Remote Sens. Environ.* **2016**, *185*, 142–154. [CrossRef] [PubMed]

56. Song, X.-P.; Huang, W.; Hansen, M.C.; Potapov, P. An evaluation of Landsat, Sentinel-2, Sentinel-1 and MODIS data for crop type mapping. *Sci. Remote Sens.* **2021**, *3*, 100018. [CrossRef]

57. Khalid, H.W.; Khalil, R.M.Z.; Qureshi, M.A. Evaluating spectral indices for water bodies extraction in western Tibetan Plateau. *Egypt. J. Remote Sens. Space Sci.* **2021**, *24*, 619–634. [CrossRef]

58. Tian, H.; Meng, M.; Wu, M.; Niu, Z. Mapping Spring Canola and Spring Wheat Using Radarsat-2 and Landsat-8 Images with Google Earth Engine. *Curr. Sci.* **2019**, *116*, 291–298. [CrossRef]